Restoring the Invisible Details in Differential Interference Contrast Microscopy Images*

Wenchao Jiang and Zhaozheng Yin

Department of Computer Science, Missouri University of Science and Technology
wjm84@mst.edu, yinz@mst.edu

Abstract. Automated image restoration in microscopy, especially in Differential Interference Contrast (DIC) imaging modality, has attracted increasing attention since it greatly facilitates living cell analysis. Previous work is able to restore the nuclei of living cells, but it is very challenging to reconstruct the unnoticeable cytoplasm details in DIC images. In this paper, we propose to extract the tiny movement information of living cells in DIC images and reveal the hidden details in DIC images by magnifying the cell's motion as well as attenuating the intensity variation from the background. From our restored images, we can clearly observe the previously-invisible details in DIC images. Experiments on two DIC image datasets demonstrate that the motion-based restoration method can reveal the hidden details of living cells, providing promising results on facilitating cell shape and behavior analysis.

1 Introduction

Automated image restoration, transforming an observed image that is challenging for direct analysis into a new image that can be effortless analyzed, has valuable applications in biological experiments, because it may make the segmentation and detection of specimens much easier and greatly facilitate the behavior analysis on specimens [1][2]. As predominantly phase objects, living cells are transparent and colorless under a traditional brightfield microscope, because they do not significantly alter the amplitude of the light waves passing through them, as a consequence, producing little or no contrast under a brightfield microscope. Differential Interference Contrast (DIC) microscopy technique (refer to Chapter 10 in [3]) has been widely used to observe living cells because it is noninvasive to cells. DIC microscopy converts the gradient of cells' optical path length into intensity variations which are visible to human.

Although the nucleus and some big organelles are visible in DIC microscopy images, there are many cell details which are not obvious in DIC microscopy images such as the cytoplasm and cell membrane, and they are difficult to be observed by human eyes. Fig.1(a) shows two DIC microscopy image patches and Fig.1(b) shows the ground truth cell mask obtained by combining the observation

* This research was supported by NSF CAREER award IIS-1351049, NSF EPSCoR grant IIA-1355406, ISC and CBSE centers at Missouri S&T.

N. Navab et al. (Eds.): MICCAI 2015, Part III, LNCS 9351, pp. 340–348, 2015.
DOI: 10.1007/978-3-319-24574-4_41

from corresponding phase contrast microscopy images. Fig.1(c) is the average segmentation mask by ten human annotators, from which we find that even humankind is likely to ignore the unnoticeable cytoplasm which spreads out into the background, but these hidden details can be informative to analyze cells' shape and behavior. In this paper, we focus on restoring the invisible (as well as visible) details in DIC microscopy images.

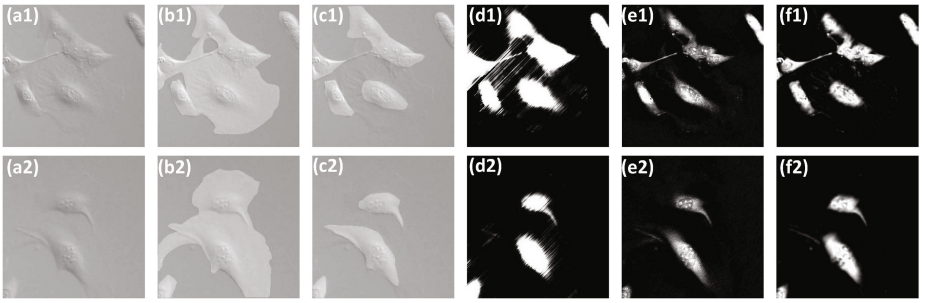

Fig. 1. Challenges in restoration of the hidden details in DIC microscopy images. (a) Two original DIC images. (b) The ground truth mask, which indicates where the cells are. (c) The mask indicates where the cells are by ten annotators merely with their naked eyes. (d) The restoration results by line integration [6]. (e) The restoration results by Wiener filter [7]. (f) The restoration results by preconditioning [8].

1.1 Related Work

The common techniques employed for microscopy image restoration include edge detection, thresholding [4], morphological operations [5]. These methods often fail when the cells are in low contrast with background. For the purpose of restoration in DIC microscopy images, lines are integrated along the shear direction inspired by the gradient interpretation property of DIC images [6], but this method introduces streaking artifacts and is sensitive to gradient noise, as shown in Fig1(d). General image processing technologies such as deconvolution by Wiener filter [7] have been investigated to restore the optical path length from DIC images. A preconditioning approach was proposed in [8] where the DIC image is reconstructed by minimizing a nonnegative-constrained convex objective function. However, neither Wiener filter nor the preconditioning method can reveal the hidden details in the DIC images and the cells are miss-segmented, as shown in Fig.1(e,f).

1.2 Our Proposal and Algorithm Overview

Although the details of living cells in a DIC image are unnoticeable by human eyes, they are likely to keep moving when we observe them in a continuous series of images, hence we are motivated to think of the following intriguing problem:

Can we extract the tiny movement information of living cells in DIC images and reveal the hidden details in DIC images by magnifying the cells' motion?

In this paper, we propose a motion-based DIC image restoration algorithm.

As shown in Fig.2, DIC image at timestamp T is to be restored. We firstly extract the spatial gradient information from every DIC image within the time sliding window $[T - \Delta t, T + \Delta t]$. The intensity values of a pixel location in the gradient images form a time-series signal and we filter it by an ideal bandpass filter to magnify small motion. The motion is further magnified in forward and backward directions independently in the temporal domain. Finally, the restoration results of two directions by motion magnification are combined to obtain the final restoration result which uncover the hidden details in the DIC image at timestamp T. Our work is different from the previous work which also considers motion information [9][10], because we do not rely on cell detection and tracking. Instead, we extract tiny motion on individual pixels and magnify it.

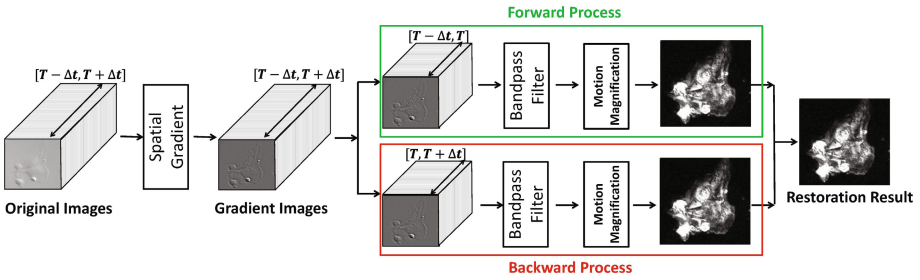

Fig. 2. Overview of our algorithm.

2 Methodology

For simplicity, we denote the original DIC image at timestamp t as $f(t)$, the pixel value of which at position (m, n) is $f(m, n, t)$. $f(T)$ is the target image to be restored at timestamp T. Let $v_m(t)$ and $v_n(t)$ denote the motion components at position (m, n) regarding to horizontal and vertical coordinates, respectively. If $f(m, n, 0) = I(m, n)$, the pixel intensity at $(m + v_m(t), n + v_n(t))$, $I(m + v_m(t), n + v_n(t))$, can be represented by image function f equivalently:

$$f(m, n, t) = I(m + v_m(t), n + v_n(t)) \tag{1}$$

By the first-order Tylor expansion, we have

$$I(m + v_m(t), n + v_n(t)) = I(m, n) + v_m(t)\frac{\partial I}{\partial m} + v_n(t)\frac{\partial I}{\partial n} \tag{2}$$

Therefore, the contrast between neighboring pixels in an image sequence (i.e., $I(m + v_m(t), n + v_n(t)) - I(m, n)$) is determined by both motion information $(v_m(t), v_n(t))$ and spatial gradient information $(\frac{\partial I}{\partial m}, \frac{\partial I}{\partial n})$. Thus we can magnify the motion by either increasing $(\frac{\partial I}{\partial m}, \frac{\partial I}{\partial n})$ or increasing $(v_m(t), v_n(t))$. This motivates us to build a Laplacian pyramid to accumulate the spatial gradient information (Subsection 2.1), design bandpass filter (Subsection 2.2) and accumulate motion information in the temporal sliding window (Subsection 2.3 and 2.4) to magnify the tiny motion caused by fine cell structures.

2.1 Gradient Images

Fig.3 illustrates the process to extract spatial gradient information from DIC microscopy images. Given a DIC image $f(t)$ (Fig.3(a)), we decompose it to several levels by the Laplacian pyramid and then reconstruct them by ignoring the last level. Fig.3(c) is the final result. Compared with the single level gradient image, such as the first level of the Laplacian pyramid in Fig.3(b), the gradient image combining several levels (Fig.3(c)) reveals more and clearer gradient information about the cells. We denote the gradient image corresponding to $f(t)$ as $g(t)$ and $g(t)$ is the input of the following motion magnification process.

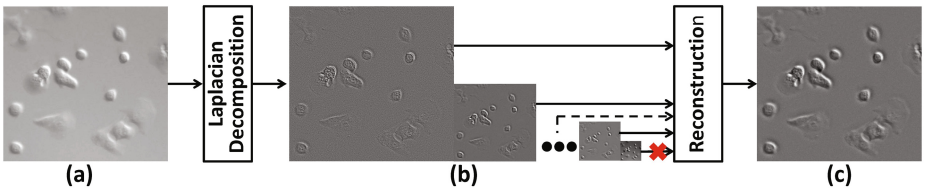

Fig. 3. Computing the gradient image $g(t)$. (a). The original image $f(t)$. (b). The Laplacian pyramid. (c). The gradient image $g(t)$.

2.2 Bandpass Filter

The original image $f(t)$ may have low signal-to-noise ratio. For example, for each image from $f(T - \Delta t)$ to $f(T + \Delta t)$, the pixel value of background is spatially stable (i.e., $(\frac{\partial I}{\partial m}, \frac{\partial I}{\partial n})$ is small on background pixels), but it can temporally change because of illumination variations, thus resulting in unwanted temporally motion in the background. Motion information $(v_m(t), v_n(t))$ can be easily extracted by the image difference of $g(t)$, but it is likely to amplify noise which is unrelated to cells' movement. We need to retain the tiny motion information of cells, meanwhile inhibiting the unwanted movement information of background pixels.

In this subsection, $g(t)$ is filtered by an ideal bandpass filter and the signal-to-noise ratio of each pixel in the temporal domain is increased. The flowchart of our bandpass filtering is shown in Fig.4 where Fig.4(a) is $g(t)$ with $t \in [T - \Delta t, T]$[1]. For each pixel (m, n), we can build a vector $g(m, n, T - \Delta t : T)$ which indicates the pixel value change at (m, n) during the time period of $[T - \Delta t : T]$. Discrete Fourier Transform (DFT) is then applied to $g(m, n, T - \Delta t : T)$ and Fig.4(b) shows examples of frequency vs. magnitude on two typical pixel locations. The principle frequency is defined as the frequency with the largest magnitude. As shown in Fig4(c), we build a principle frequency map whose pixel value at location (m, n) is the principle frequency of $g(m, n, T - \Delta t : T)$. We observe that in the cells' regions, the principle frequency is lower than that in

[1] As shown in Fig.2, the motion magnification processes towards forward and backward directions in the temporal domain are similar, thus we mainly describe the forward process in this subsection without loss of generality.

the background (presented by black regions in Fig4(c)). This is because noise variation in the background has higher frequency (fast changes) but with smaller range of variation, so people may not notice it. However, the intensity change of a pixel location caused by cell movement has lower frequency (slow changes) but with larger variation range, thus people are possible to observe cell details in continuous DIC images.

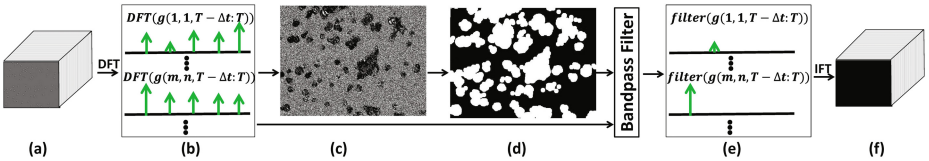

Fig. 4. Flowchart of bandpass filtering. (a) $g(t)$ with $t \in [T - \Delta t : T]$. (b) The DFT of $g(m, n, T-\Delta t : T)$. (c) Principle frequency image. (d) The bitmask by thresholding the principle frequency image, from which we can know the tentative cell and background regions. (e) Bandpass filtering result. (f) The motion image $h(t)$, which indicates the motion of each pixel.

The principle frequency map shown in Fig.4(c) inspires us to tentatively determine the cells' regions and background. We set all pixel values in the principle frequency image which are larger than the minimum of the principle frequency map as zero, yielding a bitmask that indicates the cells' regions and background as shown in Fig.4(d). The bitmask can roughly tell where the living cells are, offering us the hint on where to retain cells' tiny movement while inhibiting the motion from background noise.

For each pixel (m, n) in $g(t)$, its movement pattern may not be exactly the same during the time interval $[T-\Delta t : T]$, thus we design an ideal bandpass filter with the aid of the bitmask to keep the most salient movement of cells as well as the smallest movement in the background. The bandpass filtering increases the contrast between cell motion and background intensity variation, therefore facilitating the observation on fine details of cells.

For the tentative background regions obtained from Fig.4(d), the frequency range to be passed in the bandpass filter is set as the frequency corresponding to the *smallest* magnitude, thus all frequency components which are larger are attenuated (rejected). Note that we do not directly set all frequency components of the tentative background pixel as zero, because the tentative foreground and background segmentation in Fig.4(d) may not be accurate. For the tentative foreground regions obtained from Fig.4(d), the frequency range to be passed in the bandpass filter is set as the frequency corresponding to the *largest* magnitude, thus only the dominant frequency component related to cell motion is kept. Fig.4(e) shows the two filtering results corresponding to Fig.4(b) with the top being regarded as background and the bottom being foreground. After bandpass filtering, we apply the inverse DFT to obtain the motion images $h(t)$.

2.3 Motion Magnification

After the aforementioned processes, we obtain the motion images $h(t)$ which includes the movement information of each pixel. In this section, we further magnify the motion in a temporal sliding window to reveal cell details. This is implemented by the temporally weighted accumulation of motion. The magnification formula for forward process ($[T - \Delta t, T]$) is defined as

$$r_{fw}(T) = \sum_{t=T-\Delta t}^{T} e^{-\frac{T-t}{\Delta t}} |h(t)| \tag{3}$$

The magnification formula for backward process ($[T, T + \Delta t]$) is similarly defined as

$$r_{bw}(T) = \sum_{t=T}^{T+\Delta t} e^{-\frac{t-T}{\Delta t}} |h(t)| \tag{4}$$

where $r_{fw}(T)$ and $r_{bw}(T)$ are the motion magnified images for $f(t)$ by the forward and backward process, respectively. $e^{-\frac{T-t}{\Delta t}}$ and $e^{-\frac{t-T}{\Delta t}}$ ensure that the closer the image $h(t)$ is to the target image $h(T)$, the more contribution $h(t)$ makes to $r_{fw}(T)$ or $r_{bw}(T)$.

2.4 Combine Forward and Backward Motion Images

The final restoration image $r(T)$ for the original target image $f(T)$ can be directly defined as the elementwise min-operation on $r_{fw}(T)$ and $r_{bw}(T)$:

$$r(T) = min(r_{fw}(T), r_{bw}(T)) \tag{5}$$

As shown in Fig5(a,b,c), a cell moves from the center towards the top-right. Fig5(d,e,f) show the forward, backward and combined restoration results, respectively. In Fig5, we observe that if only one direction of motion information is used, there will be artifacts unrelated to the motion in $f(T)$. The artifacts are from the accumulated motion in the past or future DIC images. If we compute the minimum of $r_{fw}(T)$ and $r_{bw}(T)$, the artifacts are removed, leaving the cell details in the current frame only.

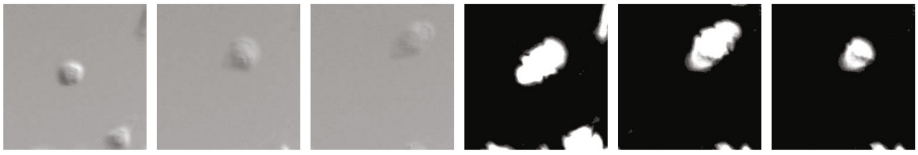

Fig. 5. Illustration of the combination of forward and backward processes.

3 Experimental Results

The proposed image restoration algorithm is tested in two different sets of Differential Interference Contrast images of 1388×1040 pixels, which were captured every 5 minutes to continuously monitor live cells. The first dataset includes 445 DIC images with each image containing about 70 cells. The second dataset includes 500 DIC images and has a wider visual field, thus each image in this dataset contains about 150 living cells. When labeling the ground truth of cell masks, we found it was likely to make mistake only with DIC images. To minimize the human errors, we took the phase contrast microscopy images on the same cell dish simultaneously when we took DIC images. Thus the ground truth was labeled by combining DIC images and corresponding phase contrast images. Δt is determined by a training dataset different from the two above-mentioned testing datasets and the following comparison on testing datasets are conducted when $\Delta t = 20$ which had the best restoration performance on the training dataset.

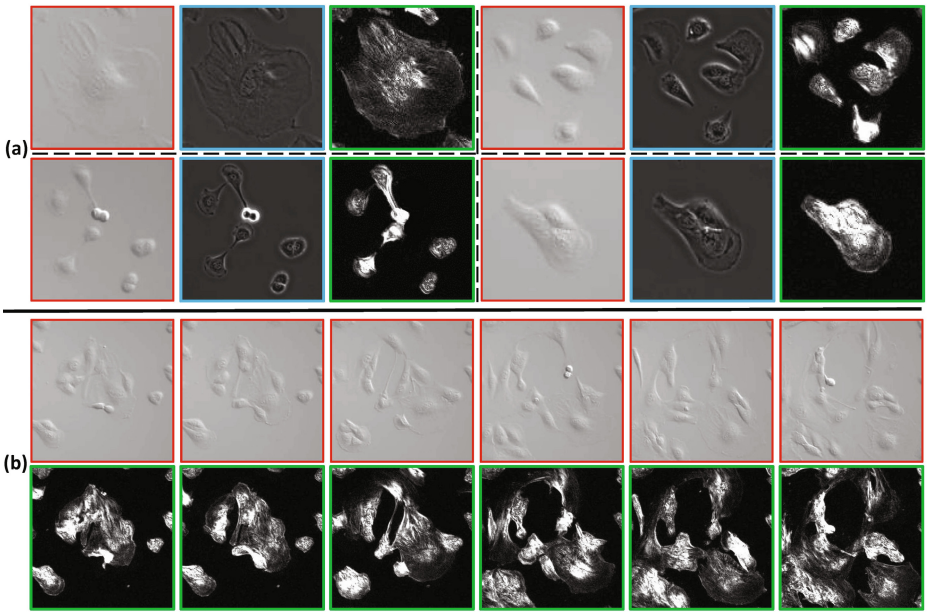

Fig. 6. The qualitative performance. (a).The images in red, blue and green boxes are the original DIC images, the corresponding phase contrast images and the restoration images obtained by the proposed algorithm, respectively. (b). The upper row shows sample DIC images during a period of 100 minutes. The bottom row is the restoration images, from which we can analyse the shape change of a cluster of cells.

3.1 Qualitative Evaluation

Fig.6 shows the qualitative performance of the proposed restoration algorithm. In Fig.6(a), the images in red or blue boxes are the original DIC images and the corresponding phase contrast images, respectively. Phase contrast images are displayed here to observe the ground truth. Unlike the previous work [6][7][8] which only reveals the nucleus of living cells (an example is in Fig.1), our approach can display the details such as the cytoplasm of living cells, even though the cytoplasm is spread out and fuses with the background (images in green boxes in Fig.6(a)). The upper row of Fig.6(b) shows some DIC images on a cluster of cells within a time interval of 100 minutes. It is clearly to observe cells' shape change and their movement, which provides more information for future cell shape and behavior analysis.

3.2 Quantitative Evaluation

The restored image enables us to achieve the cell segmentation simply using a global thresholding. Fig.7 shows the recall vs. precision curves by trying all possible thresholds for four methods: our proposed approach, line integration [6], Wiener filter [7] and preconditioning [8]. For each threshold, TP is the number of true positive pixels. FP is the number of false positive pixels. FN is the number of false negative pixels. Thus precision is defined as Precision=TP/(TP+FP) and recall is defined as Recall=TP/(TP+FN). Fig.7 shows that our proposed algorithm greatly outperforms other approaches since we can restore cell's fine details in addition to the nucleus.

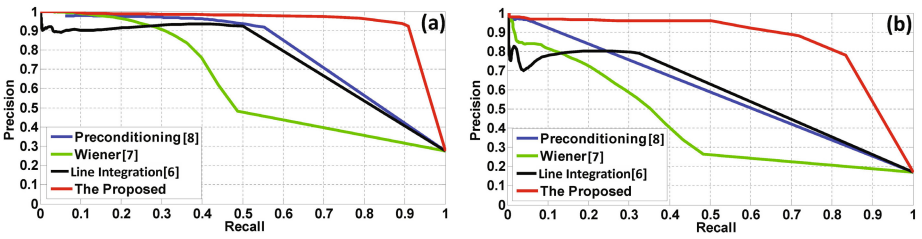

Fig. 7. The recall vs. precision comparison with other approaches. (a). Comparison in Dataset 1. (b).Comparison in Dataset 2.

4 Conclusion

In this paper, we propose a novel motion-based DIC image restoration algorithm. The tiny motion of each cell pixel is magnified by filtering a time-series of gradient signals on the pixel location using an ideal bandpass filter, while the intensity variation on the background pixels is attenuated. The motion information of a target image is further magnified by a weighted sum of a series of motion images from time-lapse image sequences. From our restored images, we can clearly

observe the previously-invisible details in DIC images. The restored images facilitate the cell segmentation greatly compared to three other image restoration methods. In the future, we will further explore cell image analysis tasks based on our restoration algorithm such as the cell proliferation event detection.

References

1. Yin, Z., Ker, D.F.E., Kanade, T.: Restoring DIC Microscopy Images from Multiple Shear Directions. In: Székely, G., Hahn, H.K. (eds.) IPMI 2011. LNCS, vol. 6801, pp. 384–397. Springer, Heidelberg (2011)
2. Kaakinen, M., et al.: Automatic Detection and Analysis of Cell Motility in Phase contrast Time lapse Images Using a Combination of Maximally Stable Extremal Regions and Kalman Filter Approaches. Journal of Microscopy (2014)
3. Murphy, D.B.: Fundamentals of Light Microscopy and Electronic Imaging. John Wiley & Sons (2001)
4. Neumann, B., et al.: High-throughput RNAi Screening by Time-lapse Imaging of Live Human Cells. Nature Methods (2006)
5. Li, K., et al.: Cell Population Tracking and Lineage Construction with Spatiotemporal Context. Medical Image Analysis (2008)
6. Kam, Z.: Microscopic Differential Interference Contrast Image Processing by Line Integration (LID) and Deconvolution. Bioimaging (1998)
7. Heise, B., Sonnleitner, A., Klement, E.P.: DIC image Reconstruction on Large Cell Scans. Microscopy Research and Technique (2005)
8. Li, K., Kanade, T.: Nonnegative mixed-norm preconditioning for microscopy image segmentation. In: Prince, J.L., Pham, D.L., Myers, K.J. (eds.) IPMI 2009. LNCS, vol. 5636, pp. 362–373. Springer, Heidelberg (2009)
9. Liu, K., et al.: Optical Flow Guided Cell Segmentation and Tracking in Developing Tissue. In: International Symposium on Biomedical Imaging (2014)
10. Hennies, J., et al.: Cell Segmentation and Cell Splitting Based on Gradient Flow Tracking in Microscopic Images. Springer, Heidelberg (2014)